



## Adsorption of bisphenol A (BPA) from aqueous solution onto mesoporous carbon and Fe-modified mesoporous carbon

Yuwei Li<sup>a</sup>, Qingwen Chai<sup>a</sup>, Jiaman Li<sup>a</sup>, Fang Liu<sup>a,b,\*</sup>, Yongqiang Wang<sup>a,b</sup>, Chaocheng Zhao<sup>a</sup>

<sup>a</sup>College of Chemical Engineering, China University of Petroleum, Qingdao 266580, China, email: liufangfw@163.com (F. Liu)

<sup>b</sup>State Key Laboratory of Petroleum Pollution Control, Beijing 102206, China

Received 20 August 2018; Accepted 25 December 2018

### ABSTRACT

Bisphenol A (BPA), as a typical representative of endocrine disrupting compounds, is extensively detected in aqueous solutions and poses a serious threat to human health. Adsorption is one of the most effective and simple way to remove bisphenol A in aqueous solutions. In this study, the mesoporous carbon (MC) material and the iron-modified mesoporous carbon material (Fe/MC-x (x: 0.5, 1, 1.5)) were prepared via one-step hydrothermal synthesis method. The textural properties of MC and Fe/MC-x were characterized using transmission electron microscopy, X-ray diffractometer, Fourier transform infrared spectrometer and N<sub>2</sub> adsorption-desorption. Several influencing factors were conducted to investigate the adsorption performance. In addition, the mechanism for the adsorption was explained via investigating the characterization part, adsorption isotherms, thermodynamics and kinetics, thoroughly. When the optimal parameters of temperature, BPA initial concentration, adsorbent dose and contact time were 25°C, 100 mg/L, 10 mg and 3 h, respectively, the maximum adsorption capacity of Fe/MC-0.5 could reach 451.6 mg/g. The adsorption equilibrium of MC and Fe/MC-x could be reached in 15–20 min. Compared with MC, the adsorption capability of Fe/MC increased by 178.5%, and the saturation time shorter up to 25%. Furthermore, the BPA adsorption on MC and Fe/MC were well in accordance with the Freundlich isotherm model ( $R^2 > 0.99$ ) while the kinetic data were best described by the pseudo-second-order kinetic model ( $R^2 > 0.99$ ). The adsorption process was a spontaneous exothermic reaction. The adsorption mechanism is mainly chemisorption of hydrogen bonding or  $\pi$ - $\pi$  stacking interactions.

*Keywords:* Mesoporous carbon; Fe-modified mesoporous carbon; Adsorption; Bisphenol A

### 1. Introduction

Endocrine disrupting compounds (EDCs) are chemical exogenous substances that interfere with the endocrine system. It enters the human body in some way and can be combined with the corresponding hormone receptors in the human body, causing hormones naturally secreted by the human body cannot be accepted by the hormone receptors and disturb with the secretion of normal hormones in the human body [1,2]. Thereby, EDCs can destroy the coordination and stability of human body environment, affecting the reproduction, nerve and development of human body [3,4].

Bisphenol A (BPA), also known as 2,2-bis(4-hydroxyphenyl) propane, as one of the most extensively used endocrine disruptor, provides a monomeric material primarily for the production of polysulfone resin, epoxy, polyphenylene oxide and other polymer materials [5–7]. It can also be applied for fine chemical products such as plasticizers, flame retardants, heat stabilizers, paints and so on. It can be detected in the wastewater of petrochemical industry, coking, plastic, mechanical manufacturing and other industries [3]. However, bisphenol A is difficult to biodegrade, resistant to chemical oxidation, low volatility, high toxicity and even very low concentration can lead to great harm to human beings, animals and

\* Corresponding author.

plants. Furthermore, it can induce liver damage, normal cell dysfunction, sexual dysfunction and cancer, which seriously threaten the life and health of human beings, are typical refractory phenolic substances. Therefore, an effective and cheap method for rapid removal of bisphenol A from aqueous solution is of great practical significance herein.

There are various methods to remove bisphenol A in the contaminated water, including adsorption [8–11], electrochemical processes [12–14], photo-degradation technology [15] and biological treatment [16–18]. However, BPA is difficult to biodegrade completely because of their toxicity to microorganisms. For example, application of biological treatment is limited. Although the electrochemical processes and photo-degradation technology may effectively removal BPA in some way, use of such processes is limited due to their high cost and small-scale application [19]. In the actual environment, photo-degradation technology is mostly unable to be applied due to the unstable degradation effect and single object of purification. Compared with these limited applications, adsorption [20–22] is considered as an optimal method owing to its simple operation, high efficiency and economic, and widely used in the treatment of BPA containing wastewater [8,23]. In fact, the key to adsorption process is the selection of adsorbents. Over the past few years, researchers have strived to research for an appropriate adsorbent for BPA with large specific surface area, reusability and production feasibility. So far, the adsorbents, such as molecular sieve, activated carbon and mesoporous carbon material [24], are all befitting adsorbents for the adsorption of bisphenol A. These advantages, such as low capital cost, high removal efficiency and dose do not produce toxic intermediates than the BPA itself [25], make molecular sieve and activated carbon the promising adsorbents. The adsorption efficiency of BPA onto adsorbents is affected by the molecular mass and size of the adsorbed substance [26]. Therefore, most adsorbents may be difficult to be penetrated by BPA micropores owing to the predominance of micropores (<2 nm). In contrast to these adsorbents, however, mesoporous carbon materials possess the large specific surface area, suitable pore volume and pore size, well-ordered and nontoxicity [27], hence have considerable adsorption capacity and better performance than other adsorbents. Mesoporous carbon materials with moderate size and uniform pore diameter facilitate the diffusion and adsorption of pollutants in the pores [28]. It also has high mechanical stability and chemical stability [29]. These characteristics make mesoporous carbon materials as optimal adsorbents. In addition, zero-valent iron attracts a lot of attention from the researchers due to its efficient reduction, adsorption and micro electrolysis [30]. Different properties of modified mesoporous carbon adsorbents are obtained via the functionalized modification of mesoporous carbon materials and the introduction of different functional groups on their surfaces and channels [31–33], which helps to improve the adsorption capacity. In order to improve the adsorption properties of polymeric adsorbents, many scientists have devoted on chemical modification because van der Waals interaction is the main force to drive BPA molecules from bulk solution to the adsorbent phase [34]. There have been many reports for the removal of BPA using modified mesoporous carbon materials; however, to the best of our knowledge, few of them researched the Fe-modified mesoporous carbon.

Hence, Fe/MC- $x$  ( $x$ : 0.5, 1, 1.5) is a hopeful candidate to deal with BPA.

Herein a simple method of approach to synthesize iron-modified Fe/MC- $x$  is a direct one-step hydrothermal treatment [35,36] with three different iron–phenol molar ratios ( $x$  is iron–phenol ratio: 0.5,1,1.5). The mesoporous carbon (MC) was prepared by the hydrothermal synthesis [37]. F127 was employed as the template, and  $\text{Fe}(\text{NO}_3)_3 \cdot 9\text{H}_2\text{O}$  was used as the iron source. This method has the characteristics of stable preparation, simple operation, economic, practical and so on. The MC and Fe/MC were characterized through X-ray diffractometer (XRD), Fourier transform infrared spectrometer (FT-IR), transmission electron microscopy (TEM) and Brunauer–Emmett–Teller (BET). The adsorption behavior of BPA onto iron-modified materials is investigated via adsorbent dose, contact time and initial concentration by comparing with MC. Kinetic theory was researched to explain the adsorption principle of BPA. The adsorption isotherms were conducted to determine the preferred isotherms. Besides, adsorption thermodynamics was also investigated.

## 2. Experimental section

### 2.1. Materials

Pluronic copolymer F127 ( $\text{PEO}_{106}\text{PPO}_{70}\text{PEO}_{106}$ , analytical pure) was obtained from Sigma-Aldrich company, USA. Bisphenol A (BPA, the purity of 97%), citric acid monohydrate ( $\text{C}_6\text{H}_8\text{O}_7 \cdot \text{H}_2\text{O}$ , analytical pure), nine hydrated iron nitrate (analytical pure), resorcinol ( $\text{C}_6\text{H}_6\text{O}_2$ , analytical pure) were bought from Sinopharm Chemical Reagent Co., Ltd. (Shanghai, China). Nitrogen ( $\text{N}_2$ , high purity) was provided by Qingdao Tianyuan gas (Shandong, China). Anhydrous ethanol ( $\text{CH}_3\text{CH}_2\text{OH}$ , analytical pure) and formaldehyde ( $\text{CH}_2\text{O}$ , analytical pure) were procured from West Long Chemical Co., Ltd. (Guangzhou, China).

### 2.2. Preparation of MC and Fe/MC

The MC was obtained using the hydrothermal synthesis method [38]. Briefly, 2.3 g of resorcinol and 1.5 g F127 was dissolved in 20 mL of deionized water and 20 mL of anhydrous ethanol. 2.3 g of citric acid monohydrate was then added to the above solution, magnetic stirring was carried out for 1 h until completely dissolved. Afterwards, 2.5 g of 37 wt% methanol solution was added dropwise into the mixture under stirring, and the mixture was stirred for 1 h. The final mixture was transferred into a 100 mL hydrothermal reactor and heated at 130°C for 10 h. The amorphous precipitate was separated by centrifugation, washed with deionized water to remove alcohol, and dried in a vacuum oven at 100°C for 10 h. The MC was obtained via calcining in a tube furnace from room temperature to 700°C with a heating rate of 1°C/min for 3 h under nitrogen atmosphere.

Iron-modified mesoporous carbon (Fe/MC) was synthesized using direct modification method [39]. At the initial step of preparing MC, resorcinol and F127 were added. At the same time, 0.42, 0.85 and 1.26 g (corresponding to the molar ratio of iron–phenol were 0.5, 1, 1.5), respectively, of  $\text{Fe}(\text{NO}_3)_3 \cdot 9\text{H}_2\text{O}$  were put into the mixture. The subsequent steps proceeded as the same as MC, and the three kinds of solid were designated as Fe/MC- $x$  ( $x$  = 0.5, 1, 1.5).

### 2.3. Characterization of MC and Fe/MC

TEM (JEM-2010UHR) image was used to observe the structure of MC and Fe/MC-x and the distribution of the loaded material. The samples are carefully lapped, added a small amount of ethanol, ultrasonic processed into suspension, and dispersed on the copper network analysis and test. The physicochemical properties of the samples were analyzed using the BET (Micromeritics ASAP2000, China) method using N<sub>2</sub> adsorption–desorption isotherms at liquid nitrogen temperature of 77 K. Before the measurement, the samples were degassed at 250°C for 8 h. The specific surface area was calculated via the BET method. The pore volume and pore diameter distributions [40] were derived from the isotherms of desorption branches using Barrett–Joyner–Halenda method. The structure of the sample was recorded on a Bruker (Beijing) Technology Co., Ltd., (Haidian District) D8 Advance XRD operating at 40 kV tube voltage and 40 mA tube flow and using Cu K $\alpha$  radiation ( $\lambda = 1.5406 \text{ \AA}$ ), Ni filter. Low-angle XRD scanned in a  $2\theta$  range of  $0.5^\circ$ – $10^\circ$ , wide-angle XRD scanned in a  $2\theta$  range of  $5^\circ$ – $75^\circ$ . The functional groups on surface of the samples were detected using a Fourier transform infrared spectrometer (FT-IR, NICOLET company (Beijing, China), NexuS870) in the range of  $400$ – $4,000 \text{ cm}^{-1}$ . The sample and KBr was ground and pressed together, and KBr was a blank background.

### 2.4. BPA adsorption and desorption experiments

The adsorption experiments of BPA were conducted using a batch system. Different adsorption conditions, such as adsorbent dosage (10–30 mg), initial concentration (20–100 mg/L), contact time (1–180 min) and reaction temperature ( $25^\circ\text{C}$ – $45^\circ\text{C}$ ), on the removal efficiency of BPA were investigated. All batch adsorption experiments were performed in a series of 250 mL conical flask filled with 100 mL of BPA solution. The MC and Fe/MC were added to conical flask and oscillated on a constant temperature water bath shaker. After each adsorption equilibrium, the solution was obtained by filtering. The final BPA concentration was measured by ultraviolet spectrophotometer at 276 nm. In addition to the effect of reaction temperature and contact time on the adsorption experiment, all the other experiments were carried out under the operating conditions at  $25^\circ\text{C}$  for 3 h. The adsorption capacity was calculated according to the following equations:

Equilibrium adsorption capacity [41]:

$$Q_e = \frac{(C_0 - C_e)V}{m} \quad (1)$$

Adsorption capacity at time  $t$  [28]:

$$Q_t = \frac{(C_0 - C_t)V}{m} \quad (2)$$

Removal percentage:

$$R = \frac{C_0 - C_e}{C_0} \times 100\% \quad (3)$$

where  $C_0$ ,  $C_e$  and  $C_t$  (mg/L) are the initial, equilibrium and at time  $t$  concentrations of the MC and Fe/MC in the solution, respectively,  $V$  (mL) is the solution volume,  $m$  (mg) is the quality of the MC and Fe/MC.

For the desorption studies, the adsorbents were separated from BPA solution and washed with deionized water to remove the excess of BPA. Afterwards, the samples were treated with 100 mL of deionized water, ethanol solution, 0.1 M HCl and 0.1 M NaOH solution to elute the adsorbed BPA on a constant temperature water bath shaker at  $25^\circ\text{C}$  for 6 h. The solution was obtained through filtering and the final BPA concentration was measured by ultraviolet spectrophotometer at 276 nm. The desorption percentage ( $R_D$ ) was calculated as:

$$R_D(\%) = \frac{\text{Concentration of desorbed BPA by eluent}}{\text{Initial concentration of BPA adsorbed on the adsorbent}} \times 100\% \quad (4)$$

## 3. Results and discussion

### 3.1. Characterization of MC and Fe/MC

TEM images of MC and Fe/MC are shown in Fig. 1. The nanopore morphology of materials can be directly observed via TEM images, and thus the pore size, pore structure of the order and the situation of surface load are judged. From the images, the darker portion of the color is pore wall, and the lighter part is pore channel. The pore channels of the MC and Fe/MC are wormlike, most of them are disordered structures [42] and the pore sizes are relatively uniform. This increases the specific surface area of the samples and facilitates the process of adsorption. Compared with MC, the black spots of iron species on Fe/MC are clearly visible, and the dispersion of the black spots is more uniform. With the increase of the proportion of iron–phenol, the density of the black spots increases. It shows that the Fe species are successfully loaded into the MC by modified behavior, and no agglomeration. The capacity of doping iron increases with the increase of the amount of iron. The degree of regularity of Fe/MC is lower than that of MC after the doping of iron. This result shows that the introduction of iron source in the one-step process participates in the prepolymer polymerization process [39], affecting the orderly polymerization of the material according to the template, and hence results in the damage of the material structure.

Fig. 2 presents nitrogen adsorption–desorption isotherms and pore size distribution curves of MC and Fe/MC. The hysteresis loops of MC and Fe/MC belong to type IV adsorption isotherms according to the classification of IUPAC adsorption isotherms. That is, the low relative pressure is mainly monolayer adsorption, followed by multi-layer adsorption, and finally the outer superficial sorption, which indicates that the iron-modified mesoporous carbon does not destroy the mesoporous structure. A distinct type H<sub>2</sub> hysteresis loop (from 0.4 to 0.7) is appeared in all four adsorbents, indicating the presence of slit-shaped intercrystallite mesopores [43]. During the adsorption process, the adsorption under low pressure is related to the monolayer adsorption, and the monolayer adsorption is reversible, so there is no hysteresis loop in the low-pressure region. However, in the middle and

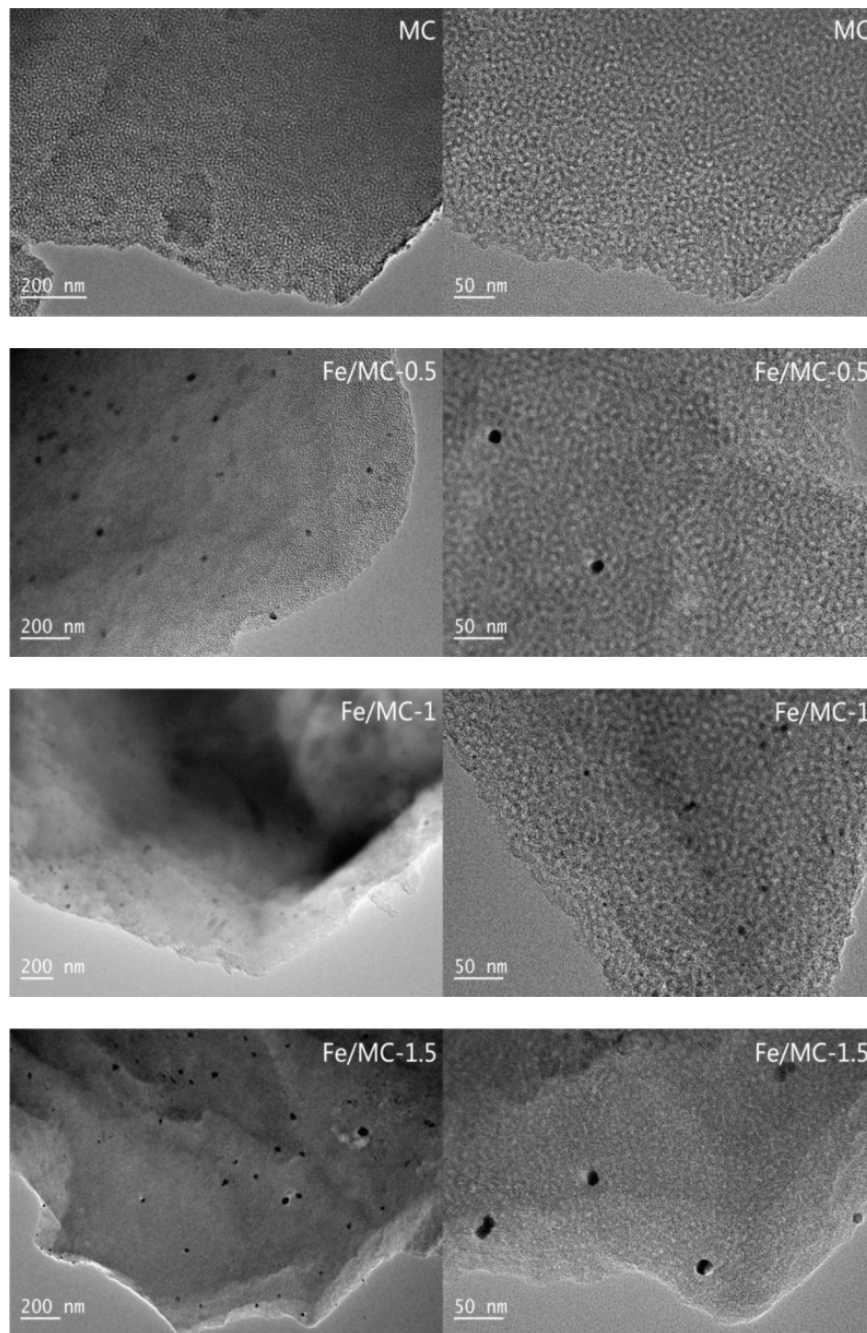


Fig. 1. TEM images of MC and Fe/MC.

high-pressure region, the desorption vapor pressure is different from the saturation pressure during adsorption, resulting in the adsorption–desorption curve that does not coincide, thus forming the  $H_2$  hysteresis loop [44]. In addition, the adsorption isotherm appears sharp jump, and the amount of uptake of nitrogen decreases with the increase of iron content. This is due to the capillary agglomeration of mesopores generated during the adsorption process, which makes the patency of channel less. The distributions of pore size of MC and Fe/MC are relatively narrow and uniform, focusing on 3–4 nm, indicating that the pore size has changed a certain degree [45].

The pore size distribution curves clearly show that the pore size of MC is mainly around 3.44 nm, while the Fe/MC is 3.51, 3.50 and 3.17 nm, respectively. Examining the textural properties of MC and Fe/MC-x, including the pore size, pore volume and specific surface area (Table 1) shows that pore volume and pore size have little change. MC has the largest pore volume of 0.24  $\text{cm}^3/\text{g}$  and the largest specific surface area of 644  $\text{m}^2/\text{g}$ , Fe/MC-0.5 possesses a maximum pore size of 3.51 nm. The parameters of Fe/MC-1.5 are the smallest, which is consistent with the nitrogen adsorption–desorption isotherm. The specific surface area of the modified material is correspondingly reduced, which may be due to the addition

of the iron species makes some channels clogged and even collapsed, resulting in a slight decrease in the specific surface area [46].

Low-angle X-ray diffraction patterns of MC and Fe/MC are used to determine the order of the samples (Fig. 3). The low-angle XRD spectra of mesoporous carbon materials before and after modification are similar, indicating that the pore structure is resemblance. All samples present only one apparent peak at  $2\theta = 1^\circ$  [47], and the peak intensity decreases after the introduction of Fe. It shows that the channel regularity of the iron-modified material decreases, and the mesoporous carbon and its modified materials have no obvious ordering, and which is in accordance with the results of TEM. The presumed reason [48] is that the introduction of iron species during modification participates in the assembling process of template and phenolic resin prepolymer, affecting the ordering of pore structure. In addition,  $\text{Fe}(\text{NO}_3)_3 \cdot 9\text{H}_2\text{O}$  is

chosen as the iron source in the experiment.  $\text{Fe}^{3+}$  was hydrolyzed to form  $\text{H}^+$ . As a result, the addition of iron source and the amount of iron source increased, the acidity strength of the reaction system increased, the speed of phenolic condensation was affected [48], and the channels became more and more messy.

The wide-angle X-ray diffraction patterns (Fig. 4) are used to estimate the situation of introduction and the existing form of iron species in the modified materials. As the iron content increases, a new diffraction peak at  $2\theta = 44.6^\circ$  is observed in the modified materials, corresponding to the interplanar spacing of  $2.03\text{\AA}$ , which is in accordance with the (110) diffraction of  $\alpha\text{-Fe}^0$  (JCPDS card) [49]. It is indicated that the iron form supported on the mesoporous carbon after the modified behavior is nanometer zero valent iron. In the process of material synthesis, the supported iron nanoparticles can be reduced to zero-valent iron by high-temperature carbothermal reduction under inert atmosphere, and the threshold temperature is  $600^\circ\text{C}$  [39,50]. In this experiment, MC and Fe/MC are synthesized through high-temperature carbothermal reaction under the temperature as high as  $700^\circ\text{C}$ . During the high-temperature carbothermal reaction of carbon source and iron nitrate particles, the introduced trivalent iron particles are reduced to zero valent iron. The weak diffraction peaks of iron may be due to the insufficient addition of total iron.

The Fourier-transform IR (FT-IR) spectra of MC and Fe/MC before (a) and after (b) adsorption are used to measure the structural composition and chemical groups of the

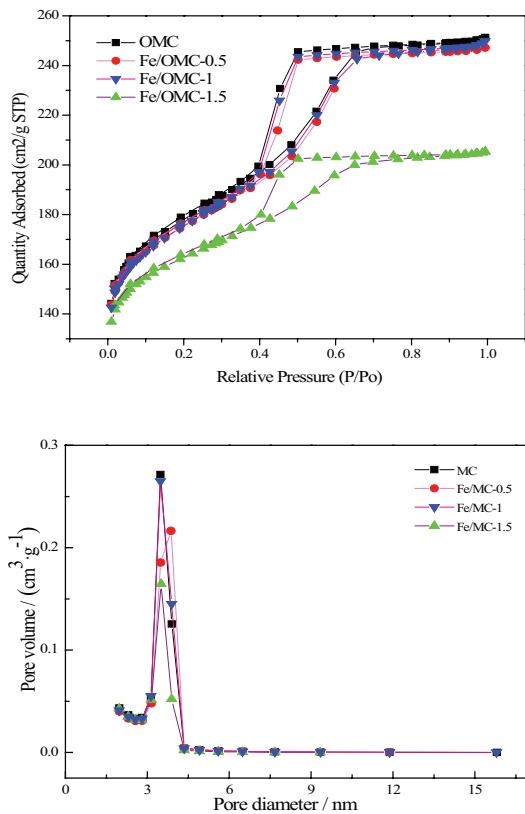


Fig. 2. Nitrogen adsorption–desorption isotherms and pore size distribution curves of MC and Fe/MC.

Table 1  
Textural properties of MC and Fe/MC

Material	Pore size (nm)	Pore volume ( $\text{cm}^3/\text{g}$ )	Specific surface area ( $\text{m}^2/\text{g}$ )
MC	3.44	0.24	643.64
Fe/MC-0.5	3.51	0.23	635.63
Fe/MC-1	3.50	0.24	636.07
Fe/MC-1.5	3.17	0.15	587.26

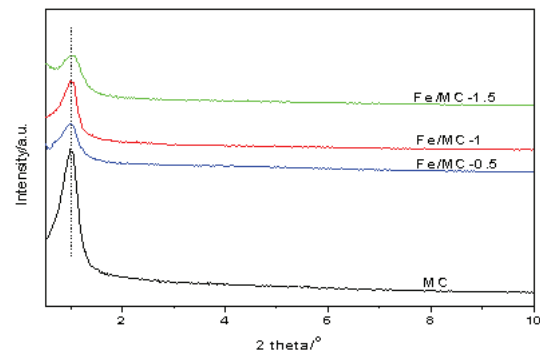


Fig. 3. Low-angle XRD patterns of MC and Fe/MC.

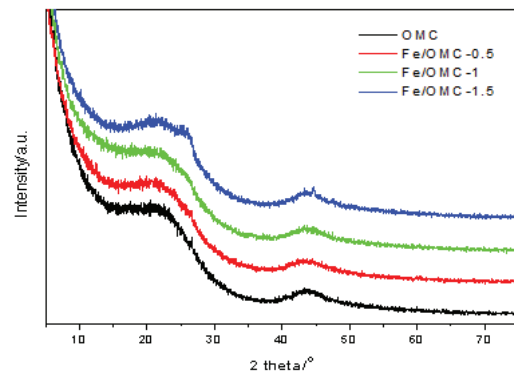


Fig. 4. Wide-angle XRD patterns of MC and Fe/MC.

samples (Fig. 5). For MC and Fe/MC, the band near  $3,437\text{ cm}^{-1}$  corresponds to stretching vibration peak of O–H group, the peaks at  $2,900$  and  $2,800\text{ cm}^{-1}$  are attributed to the stretching vibration peak of C–H group, the peak at  $1,746\text{ cm}^{-1}$  is due to stretching vibration peak [51] of C=O. The stretching vibration [52] band of aromatic ring is between  $1,650$  and  $1,500\text{ cm}^{-1}$ . The C–O–C symmetrical stretching vibration peak and stretching vibration of C–O as well as bending vibration of O–H give rise to bands between  $1,300$  and  $1,000\text{ cm}^{-1}$ . The absorption of Fe/MC is more obvious than that of MC in the above band. It is shown that the modification of Fe makes the oxygen-containing functional groups on the surface of the mesoporous carbon material increase correspondingly, and thus increasing the polarity of the surface of the mesoporous carbon material. This is beneficial to the adsorption capacity of the material.

Compared with MC, iron-modified materials appear through some new peak in the spectrum. The peak at  $1,418\text{ cm}^{-1}$  indicates the presence of characteristic absorption peak of Fe. Many new absorption peaks appear in the spectrum below  $900\text{ cm}^{-1}$ , and the intensity of these peaks enhances correspondingly with the increase of the addition of iron. It is known that the physical adsorption process only changes the displacement and intensity of the characteristic absorption bands of the original adsorptive molecules, and does not produce a new characteristic peak. Therefore, it is inferred that there is chemisorption after Fe modification of the mesoporous carbon material, resulting in a new absorption peak.

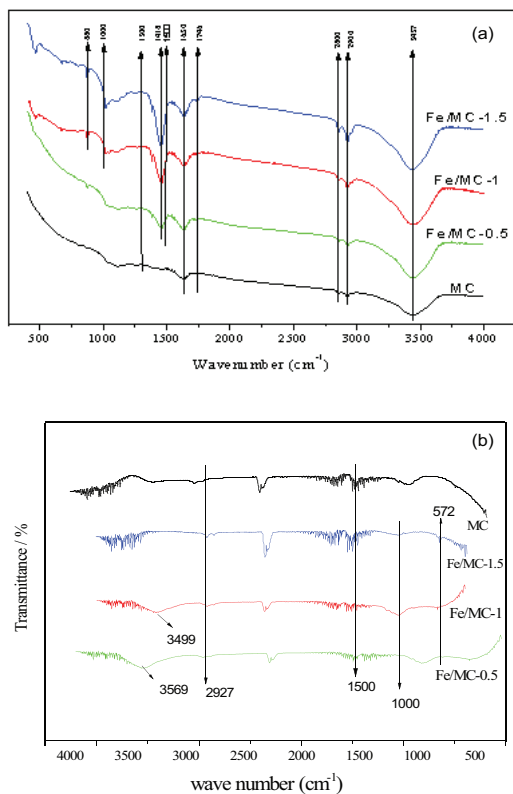


Fig. 5. FT-IR spectra of MC and Fe/MC (a) before and (b) after adsorption.

After BPA adsorption (Fig. 5(b)), the stretching vibration peak of O–H group has a shift from  $3,437$  to  $3,499$  and  $3,569\text{ cm}^{-1}$  after adsorption, which could be attributed to the hydrogen bonding between hydroxyl groups in both Fe/MC and BPA [30]. Meanwhile, the new characteristic peaks of BPA at  $2,800$ – $3,000$  and  $500$ – $1,800\text{ cm}^{-1}$  are recommended in the FT-IR spectra of MC and Fe/MC after BPA adsorbed, which turns out that a great deal of BPA molecules are adsorbed onto the MC and Fe/MC. The peaks at  $1,500\text{ cm}^{-1}$  in the Fe/MC are attributed to the stretching vibrations of aromatic C=C, and it shifts a little after adsorption, indicating that there might be the  $\pi$ – $\pi$  interaction between the benzene rings of BPA and Fe/MC planes [52].

In order to better explain the adsorption properties of MC and Fe/MC, the SEM images after adsorption are used to estimate the change of the surface morphology (Fig. 6). From the images, the surface of MC is smoother. Obvious tiny holes are observed on the Fe/MC material, indicating that the Fe species are successfully loaded onto the MC by modified behavior. As the proportion of iron–phenol increases, the tiny holes increase and the dispersion is more uniform. Those tiny holes may increase the surface area of the MC and Fe/MC and are beneficial to the adsorption process [23]. According to the FT-IR spectra after adsorption, the MC and Fe/MC successfully adsorbed BPA molecule, therefore, it can be speculated that the white particles are BPA molecules. Compared with MC, a large number of BPA molecules are adsorbed in the tiny holes of the Fe/MC. However, with the increase of the proportion of iron–phenol increases, the structure of tiny holes changed slightly, resulting in a decrease in BPA adsorption capacity. Carbon atoms may participate in the reduction process of trivalent iron ions in the channels of MC, which may influence the structure of the tiny holes [35].

### 3.2. BPA adsorption performance of MC and Fe/MC

The effect of dose of MC and Fe/MC on the adsorption of BPA is shown in Fig. 7. Under the same experimental conditions, the BPA removal efficiency increases with the increase in adsorbent dose, and the change is not sharp. The decrease in adsorption capacity with increasing adsorbent may be due to the flux separation or the concentration gradient between BPA concentration in the solution and the BPA concentration in the adsorbent surface [53]. Obviously, the BPA removal

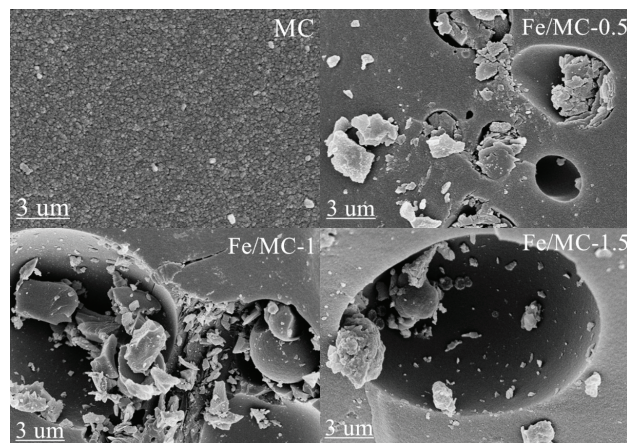


Fig. 6. SEM image of MC and Fe/MC after adsorption.

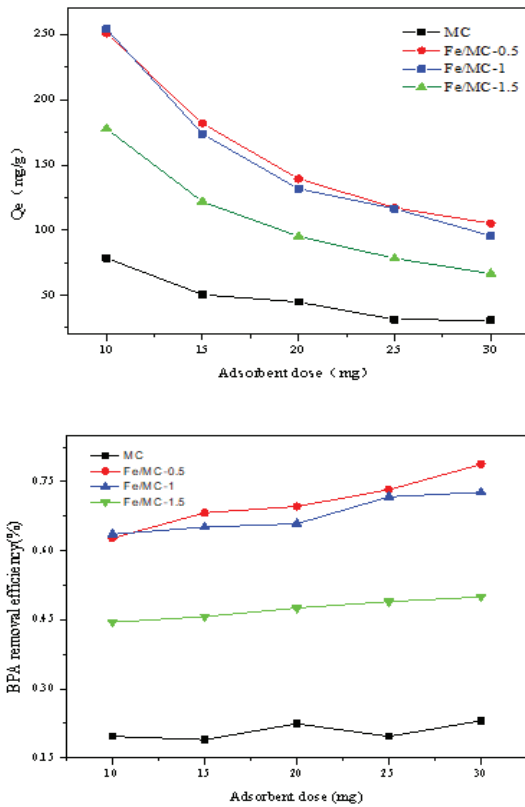


Fig. 7. Effect of adsorbent dose on MC and Fe/MC.

efficiency and adsorption capacity of Fe/MC is higher than that of MC. The size of the adsorption capacity and removal efficiency is arranged in the following order: Fe/MC-0.5  $\approx$  Fe/MC-1 > Fe/MC-1.5 > MC. The maximum adsorption capacity of each adsorbent is obtained with BPA initial concentration of 40 mg/L and the adsorbent dose of 10 mg at 25°C. Among them, the maximum adsorption capacity of Fe/MC-0.5 is 251.0 mg/g, and the corresponding removal efficiency is 78.77%. For a fixed concentration of BPA, the adsorption sites provided by the small adsorbent dose are fully utilized. However, the total available active adsorption sites are limited, easy to achieve adsorption saturation, and the adsorption sites provided by a large number of adsorbent doses are relatively more. Therefore, when the adsorbent dose is small, the adsorption capacity is large, and with the adsorbent dose increasing, the removal efficiency is increased.

Initial concentration is an important factor affecting the adsorption efficiency of BPA. In this study, the effects of different initial concentration of BPA on adsorption capacity and removal efficiency are investigated under experimental conditions, the range of initial concentration is set from 20 to 100 mg/L.

As shown in Fig. 8, the equilibrium adsorption capacity  $Q_e$  of each adsorbent increases with the increase of the initial concentration of BPA solution. The adsorption capacities of Fe/MC are higher than that of MC, and the difference between them diminishes with the increase of temperature. The size of the adsorption capacity is arranged in the following order: Fe/MC-0.5  $\approx$  Fe/MC-1 > Fe/MC-1.5 > MC. When 10 mg Fe/MC-0.5 adsorbed 100 mg/L BPA solution

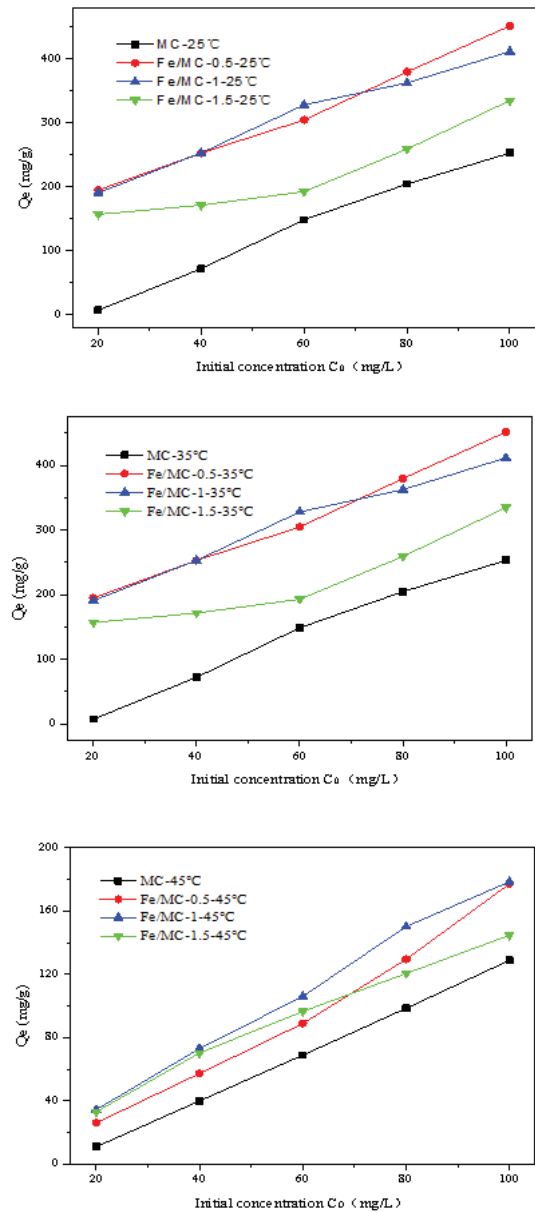


Fig. 8. Effect of BPA initial concentration at different temperature on MC and Fe/MC.

at 25°C, the maximum adsorption capacity of Fe/MC-0.5 is 451.6 mg/g. In terms of the adsorption capacity, the higher the initial concentration of BPA, resulting in the probability of collision between BPA molecules and the adsorbent is large, thereby the adsorption capacity is large. Iron-modified mesoporous carbon materials possess higher adsorption properties than mesoporous carbon materials due to the active sites of adsorption on the mesoporous carbon surface with Fe chemical bonds. With the increase of temperature, the adsorption capacity of MC and Fe/MC all decreases obviously, and the slope of each adsorption curve decreases. That is to say, the increased rate of the adsorption capacity decreases with an increase in initial concentration. When the temperature rises, the solubility of BPA in the solution increases [54], which makes the adsorption capacity of adsorbents decrease.

The main reason for this phenomenon is the decrease of physical adsorption forces [55]. Adsorption is an exothermic reaction, and high temperature is not conducive to the adsorption behavior of these adsorbents on BPA.

Another significant factor on BPA adsorption process is the contact time, which can control the amount of adsorption. Fig. 9 shows the effect of contact time on removal of BPA by the MC and Fe/MC. The adsorption capacity increases significantly with respect to contact time during the first 20 min of initial stage, and gradually slows down and tends to be stable as the adsorption equilibrium occurred at about 180 min. Therefore, under the experimental conditions, the MC can reach the adsorption equilibrium at 20 min, and the adsorption equilibrium of modified samples can be achieved in 15 min. At the beginning of the reaction, the samples have numerous and vacant active adsorption sites, the BPA molecules spread, transfer and adsorb quickly on the surface and inside of the adsorbents. With the time lapses, the number of vacancy adsorption sites reduces, resulting in a slower adsorption rate until the adsorption equilibrium is reached. Similarly, the higher the initial concentration of BPA, the greater the adsorption rate of adsorbed molecules. The reason for this is probably due to the driving force to the vacancy adsorption sites of BPA and adsorbents [56]. Both the MC and Fe/MC have larger specific area and pore volume with little difference. The larger specific surface area is beneficial to the occurrence of adsorption, thereby the adsorbents can quickly achieve the adsorption equilibrium.

### 3.3. Adsorption isotherms

In order to better explain the adsorption process of the MC and Fe/MC in the adsorbent liquid, the adsorption isotherm equations are often analyzed using Langmuir [57,58] and Freundlich [59] models.

The Langmuir isotherm model can be described by Eq. (5) as follows:

$$\frac{C_e}{Q_e} = \frac{1}{K_L Q_m} + \frac{C_e}{Q_m} \quad (5)$$

Another important dimensionless separation parameter related to the Langmuir model,  $R_L$ , could help predict the adsorption model, which is given by Eq. (6):

$$R_L = \frac{1}{1 + K_L C_0} \quad (6)$$

where  $Q_m$  (mg/g) is the maximum adsorption capacity of monolayer at equilibrium,  $K_L$  (L/mg) is the adsorption equilibrium constant, which describes the intensity of adsorption,  $R_L$  represents the nature of adsorption process, which can be grouped into irreversible adsorption ( $R_L = 0$ ), favorable adsorption ( $0 < R_L < 1$ ), linear adsorption ( $R_L = 1$ ) or unfavorable adsorption ( $R_L > 1$ ). The  $Q_m$  and intercept  $\frac{1}{K_L Q_m}$  can be obtained from slope  $\frac{1}{Q_m}$  of the plot  $\frac{C_e}{Q_e}$  against  $C_e$  of different concentrations, and  $K_L$  is calculated from  $Q_m$ .

The Freundlich model can be presented by Eq. (7):

$$\ln Q_e = \ln K_F + \frac{1}{n} \ln C_e \quad (7)$$

where  $K_F$  (mg/g) is the Freundlich affinity coefficient. Generally speaking,  $K_F$  decreases with the increasing of temperature.  $n$  is the Freundlich constant, which is related to the adsorption nature. When  $2 < n < 10$ , the adsorption reaction is easy to proceed, when  $n < 0.5$ , the adsorption is difficult to carry out [60]. The slope  $1/n$  and intercept  $\ln K_F$  can be obtained from a straight line of the plot  $\ln Q_e$  against  $\ln C_e$  of different concentrations. The parameters of adsorption isotherm according to Langmuir and Freundlich models are summarized in Table 2.

The Langmuir model assumes that the adsorption of single molecular layer is uniform. The adsorption process of heterogeneous surface distribution can be described by the Freundlich model. A  $R^2$  value of a good fitting model is supported to be at least 0.8 [61]. As shown in Table 2, all the regression models are a good description of the adsorption process of BPA. However, the adsorption data of Freundlich model fit better than that of Langmuir model, indicating that these adsorption processes belong to heterogeneous adsorption occurred in the multi-molecular layer. The  $K_F$  decreases gradually as the temperature increases, indicating that the adsorption capacity decreases with the increasing of temperature. When  $n$  is close to 0.5 at 45°C, the adsorption process is becoming more and more difficult. With the temperature increasing,  $K_L$  decreases overall. It can be seen that the adsorption is exothermic reaction, and high temperature is not favorable for the adsorption.  $0 < R_L < 1$  and  $n > 0.5$  indicates that the adsorption is a preferential adsorption, and the adsorption process is easy to carry on.

Dehghani et al. [24] showed that the isotherm data of the single-walled carbon nanotubes (SWCNTs) and multi-walled carbon nanotubes (MWCNTs) fit well with the Freundlich–Langmuir and Langmuir isotherm models ( $R^2 > 0.99$ ), respectively, and the maximum adsorption capacities of the SWCNTs and MWCNTs were 71 and 111 mg/g, respectively. Liu et al. [62] reported that the isotherm of BPA on mesoporous carbon (MC) and N-modified mesoporous carbon (NMC) obeys Freundlich isotherm model. The result reported by Cunha et al. [63] concerning Freundlich model for sorption of BPA is consistent with this study.

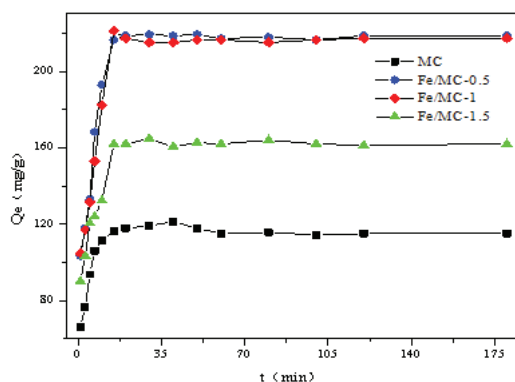


Fig. 9. Effect of contact time on MC and Fe/MC.

Table 2  
Adsorption isotherm parameters of adsorbents at different temperatures

T (°C)	Model	Adsorbent	Q <sub>m</sub> (mg/g)	K <sub>L</sub> (L/mg)	R <sub>L</sub>	R <sup>2</sup>	
25	Langmuir	MC	271.74	0.0069	0.5916–0.8787	0.7094	
		Fe/MC-0.5	462.96	0.1280	0.0725–0.2810	0.8875	
		Fe/MC-1	429.18	0.1643	0.0574–0.2333	0.9609	
		Fe/MC-1.5	354.61	0.0571	0.1490–0.4667	0.7171	
	Freundlich			K <sub>F</sub> (mg/g)	N	/	R <sup>2</sup>
		MC	0.6766	0.7220	/	0.9768	
		Fe/MC-0.5	76.1770	2.3128	/	0.9230	
		Fe/MC-1	192.5373	5.7644	/	0.9784	
		Fe/MC-1.5	3.0447	0.8949	/	0.9929	
35	Langmuir	MC	249.38	0.0039	0.7178–0.9271	0.9237	
		Fe/MC-0.5	362.32	0.0588	0.1454–0.4596	0.9477	
		Fe/MC-1	362.32	0.0270	0.2705–0.6496	0.9101	
		Fe/MC-1.5	290.70	0.0438	0.1858–0.5329	0.8969	
	Freundlich			K <sub>F</sub> (mg/g)	N	/	R <sup>2</sup>
		MC	0.9381	0.8486	/	0.9940	
		Fe/MC-0.5	39.1990	2.3422	/	0.9932	
		Fe/MC-1	28.3853	2.0484	/	0.9342	
		Fe/MC-1.5	2.9632	2.1884	/	0.9200	
45	Langmuir	MC	230.41	0.0042	0.7040–0.9224	0.8809	
		Fe/MC-0.5	335.57	0.0042	0.7058–0.9230	0.9798	
		Fe/MC-1	306.75	0.0067	0.5981–0.8815	0.8436	
		Fe/MC-1.5	800.00	0.0026	0.7910–0.9501	0.8553	
	Freundlich			K <sub>F</sub> (mg/g)	N	/	R <sup>2</sup>
		MC	0.1083	0.6222	/	0.9828	
		Fe/MC-0.5	0.7939	0.8238	/	0.9957	
		Fe/MC-1	1.8983	0.9636	/	0.9967	
		Fe/MC-1.5	2.8239	1.1185	/	0.9862	

3.4. Adsorption kinetics

In order to better evaluate the mass transfer and chemical reaction in the adsorption process, the adsorption rate and dynamic equilibrium [13], explain the adsorption principle of BPA from the kinetic point of view, pseudo-first-order kinetic model, pseudo-second-order kinetic model and the internal particle diffusion model are investigated in this study [64]. The kinetic data of adsorption are calculated based on the relationship between contact time and adsorption capacity and shown in Table 3. The model equations are as follows.

The pseudo-first-order kinetic model as a basic model based on the adsorption capacity of solid is shown in Eq. (8).

$$\ln(Q_e - Q_t) = \ln Q_e - k_1 t \tag{8}$$

where k<sub>1</sub> (min<sup>-1</sup>) is the pseudo-first-order kinetic adsorption rate constant, the theoretical Q<sub>e</sub> and k<sub>1</sub> can be obtained from the intercept and slope of the plot ln(Q<sub>e</sub> - Q<sub>t</sub>) against t.

The pseudo-second-order kinetics based on the assumption that the adsorption rate is controlled by chemisorption is as shown in Eq. (9) [64]:

$$\frac{t}{Q_t} = \frac{1}{k_2 Q_e^2} + \frac{t}{Q_e} \tag{9}$$

where k<sub>2</sub> (g/(mg min)) is the pseudo-second-order kinetic adsorption rate constant, and the initial adsorption rate h = k<sub>2</sub> · Q<sub>e</sub><sup>2</sup>, mg/(g·min). The parameters Q<sub>e</sub> and intercept  $\frac{1}{k_2 Q_e^2}$  can be obtained from the slope  $\frac{1}{Q_e}$  of the plot  $\frac{t}{Q_t}$  against t, and k<sub>2</sub> can be calculated according to Q<sub>e</sub>.

The internal particle diffusion model describing the diffusion process of BPA inside the MC and Fe/MC is applied in Eq. (10):

$$Q_t = k_i t^{0.5} + C \tag{10}$$

where  $k_i$  ( $\text{mg}/(\text{g}\cdot\text{min})^{0.5}$ ) is the intraparticle diffusion rate constant,  $C$  is the intercept, 1. The intercept  $C$  and slope  $k_i$  can be obtained from a straight line of the plot  $Q_i$  against  $t^{0.5}$ .

From Table 3, the equilibrium adsorption capacity of the MC and Fe/MC calculated by the first-order kinetic model is quite different from the actual experimental value. The correlation coefficient value of the pseudo-first-order kinetic model is around 0.8, the fitting is not ideal. That is to say, the control of the membrane diffusion step is less restrictive during the adsorption process. The correlation coefficient values of the pseudo-second-order kinetic model are better than 0.99, the fitting is preferable. In addition, the calculated equilibrium adsorption capacity is close to the actual experimental results, and it is proved once again that the adsorption kinetics of BPA on the MC and Fe/MC can be described in detail by the pseudo-second-order kinetic model. This kinetic model can be used to predict the adsorption amount of BPA at equilibrium and at different contact time intervals [65]. The adsorption mechanism lies in the electron sharing or electron transfer between the MC and Fe/MC and the BPA [66]. The adsorption process is mainly chemisorption as the step of rate control. The adsorption rates of the MC and Fe/MC are little different, and the adsorption rate of MC is the largest. The internal particle diffusion model primarily evaluates the process by which the BPA diffuses into the inner surface through the outer surface of the MC and Fe/MC. The rate of the process is related to the rate of diffusion through the pores. The correlation coefficient values of the internal particle diffusion model are about 0.87, the fitting is not good. That is, the structure of the MC and Fe/MC has little effect on the adsorption process. The internal particle diffusion is not the primary step of rate control. All the results suggest that the pseudo-second-order kinetics model better explains the

adsorption kinetics of BPA. The reaction adsorption mechanism of the pseudo-second-order kinetics model includes the diffusion and adsorption of external liquid film and the diffusion of internal particles and other all processes. The same results have been confirmed in the report of Iram et al. [67].

### 3.5. Adsorption thermodynamics

The degree and the driving force of reaction during the adsorption process are usually analyzed by thermodynamics. The thermodynamic parameters can be calculated according to the Gibbs equation (Eqs. (11)–(13)) with adsorption isotherm parameters [68]. The internal energy changes during the adsorption process can be described by three thermodynamic parameters, namely standard enthalpy ( $\Delta H$ ), standard entropy ( $\Delta S$ ) and standard free energy ( $\Delta G$ ). The obtained parameters are summarized in Table 4.

$$\Delta G = \Delta H - T\Delta S \quad (11)$$

$$\ln K_d = \frac{\Delta S}{R} - \frac{\Delta H}{RT} \quad (12)$$

$$K_d = \frac{Q_e}{C_e} \quad (13)$$

where  $K_d$  is adsorption equilibrium constant;  $R$  is ideal gas constant,  $8.314 \text{ J}/(\text{mol}\cdot\text{K})$ ;  $T$  (K) is absolute temperature;  $C_e$  ( $\text{mg}/\text{L}$ ) and  $Q_e$  ( $\text{mg}/\text{g}$ ) are the BPA concentration and adsorption capacity at equilibrium, respectively. The  $\Delta H$  and  $\Delta S$  can be obtained from a straight line of the plot  $\ln K_d$  against  $\frac{1}{T}$ .

Table 3  
Kinetic parameters of adsorbents

Model	Adsorbent	$Q_{e,\text{exp}}$ (mg/g)	$Q_{e,\text{cal}}$ (mg/g)	$K_1$ ( $\text{min}^{-1}$ )	/	$R^2$
Pseudo-first-order kinetic model	MC	119.22	43.81	0.0898	/	0.8345
	Fe/MC-0.5	219.22	125.92	0.0726	/	0.8075
	Fe/MC-1	221.19	127.20	0.0725	/	0.7103
	Fe/MC-1.5	164.74	82.60	0.0771	/	0.8549
Pseudo-second-order kinetic model		$Q_{e,\text{exp}}$ (mg/g)	$Q_{e,\text{cal}}$ (mg/g)	$K_2$ ( $\text{g}/(\text{mg}\cdot\text{min})^{-1}$ )	$h$ ( $\text{mg}\cdot(\text{g}\cdot\text{min})^{-1}$ )	$R^2$
	MC	119.22	123.92	0.0063	97.2763	0.9985
	Fe/MC-0.5	219.22	241.55	0.0016	91.4913	0.9904
	Fe/MC-1	221.19	239.81	0.0015	84.4595	0.9863
Internal particle diffusion model		$Q_{e,\text{exp}}$ (mg/g)	/	$K_i$ ( $\text{mg}/(\text{g}\cdot\text{min})^{0.5}$ )	$C$	$R^2$
	MC	119.22	/	12.1226	63.5217	0.7714
	Fe/MC-0.5	219.22	/	30.1736	78.3216	0.8587
	Fe/MC-1	221.19	/	29.8578	75.4751	0.8720
	Fe/MC-1.5	164.74	/	18.3896	75.8659	0.9111

Table 4  
Thermodynamic parameters of adsorbents

Adsorbent	T/K	$\ln K_d$	$\Delta H/(\text{kJ}\cdot\text{mol}^{-1})$	$\Delta S/(\text{J}\cdot(\text{mol}\cdot\text{K})^{-1})$	$\Delta G/(\text{kJ}\cdot\text{mol}^{-1})$
MC	298	0.2219	-32.738	-99.889	-2.971
	308	-0.2846	-32.738	-99.889	-1.973
	318	-0.3126	-32.738	-99.889	-0.974
Fe/MC-0.5	298	2.0182	-53.118	-161.283	-5.055
	308	1.5010	-53.118	-161.283	-3.442
	318	0.0971	-53.118	-161.283	-1.915
Fe/MC-1	298	1.9160	-46.254	-139.430	-4.704
	308	1.2794	-46.254	-139.430	-3.309
	318	0.3388	-46.254	-139.430	-1.8191
Fe/MC-1.5	298	-3.6262	-42.980	-130.534	-4.080
	308	1.1317	-42.980	-130.534	-2.775
	318	-0.7443	-42.980	-130.534	-1.470

$\Delta G$  is the basis for judging whether the adsorption process is spontaneous, under a certain experimental condition, the negative value of free energy indicates the adsorption process is spontaneous and feasible [69]. As shown in Table 4, the free energy and entropy value of the MC and Fe/MC are all negative, indicating that the adsorption process is spontaneous and exothermic reaction in nature. The  $\Delta G$  values of modified mesoporous carbon become more negative with decrease in reaction temperature, which suggests that the BPA adsorption process on the MC and Fe/MC is more spontaneous and favorable at lower temperatures. Furthermore, the negative values of  $\Delta H$  confirm the exothermic nature of BPA [70]. These are consistent with the analysis of the adsorption isotherm. The negative value of  $\Delta S$  confirms that the affinity of the MC and Fe/MC for BPA and reflects a decreasing of disorder or randomness on the solid–solution interface during the process of adsorption. In addition, when the increase amount of iron in mesoporous carbon, the entropy value gradually increases, indicating that the disorder of the material increases. This agrees with the conclusion of the TEM.

The enthalpy value during adsorption process is usually used to distinguish whether reaction is physical or chemical adsorption. Oepen et al. [71] reported the adsorption heat range of different forces. Among them, van der Waals force (including dispersion force, induction force and orientation force) is about 2–29 kJ/mol, hydrogen bonding force is 2–40 kJ/mol, ligand exchange force is about 40 kJ/mol, dipole force is 2–29 kJ/mol, chemical bond force is greater than 60 kJ/mol. The range of  $\Delta H$  is 25–59 kJ/mol, indicating that physical adsorption and chemisorption exists simultaneously in the adsorption process of the MC and Fe/MC. During the adsorption process, the adsorption force of Fe/MC-0.5 and Fe/MC-1 is between the ligand exchange force and the chemical bond force, MC may mainly exists the hydrogen bonding force, and the Fe/MC-1.5 may exist the ligand exchange force. Therefore, the adsorption of the MC and Fe/MC on BPA is the result of synergetic effect of the ligand exchange force, the hydrogen bonding force and the dipole force, all of which are strong forces. This process indicates

that physical adsorption and chemisorption may exist at the same time, but the performance of physical adsorption is not obvious, mainly manifests as chemical reaction. The enhanced chemical adsorption capacity not only compensates for the physical loss caused by the decrease in specific surface area and pore volume but also greatly improves the total adsorption capacity. Physical adsorption is often a preparatory stage for chemisorption.

### 3.6. Desorption and comparison studies

The application prospective of any adsorbent is a significant value because the adsorbent could be more valuable and competitive if it can be used for multiple cycles of adsorption. Here, the desorption accessibility of the MC and Fe/MC for the removal of BPA from aqueous solution was explored. The desorption test by deionized water, ethanol solution (75%, v/v), 0.1 M HCl and 0.1 M NaOH solution is carried out. From Fig. 10, it can be found that the desorption of BPA is better in ethanol solution. The better recovery of BPA in ethanol solution is that BPA belongs to liposoluble substance. Therefore, ethanol solution can be used as a cost-effective eluant to remove BPA from the MC and Fe/MC.

To investigate the competitiveness, a comparison of the monolayer adsorption capacity of the MC and Fe/MC toward BPA with the reported different adsorbents is shown in Table 5. The maximum monolayer adsorption capacity of the Fe/MC-0.5 is higher than other obtained for the largest number of adsorbents. Furthermore, since the use of any other flocculant is not essential, little secondary pollution is introduced into aqueous solution during the adsorption process. Therefore, the Fe/MC-0.5 can be considered as one of the highly efficient adsorbents to remove BPA from aqueous solution.

### 3.7. Adsorption mechanism

The adsorption mechanisms of the MC and Fe/MC toward BPA are inferred based on the preceding FTIR, SEM, adsorption kinetics, adsorption isotherm and adsorption

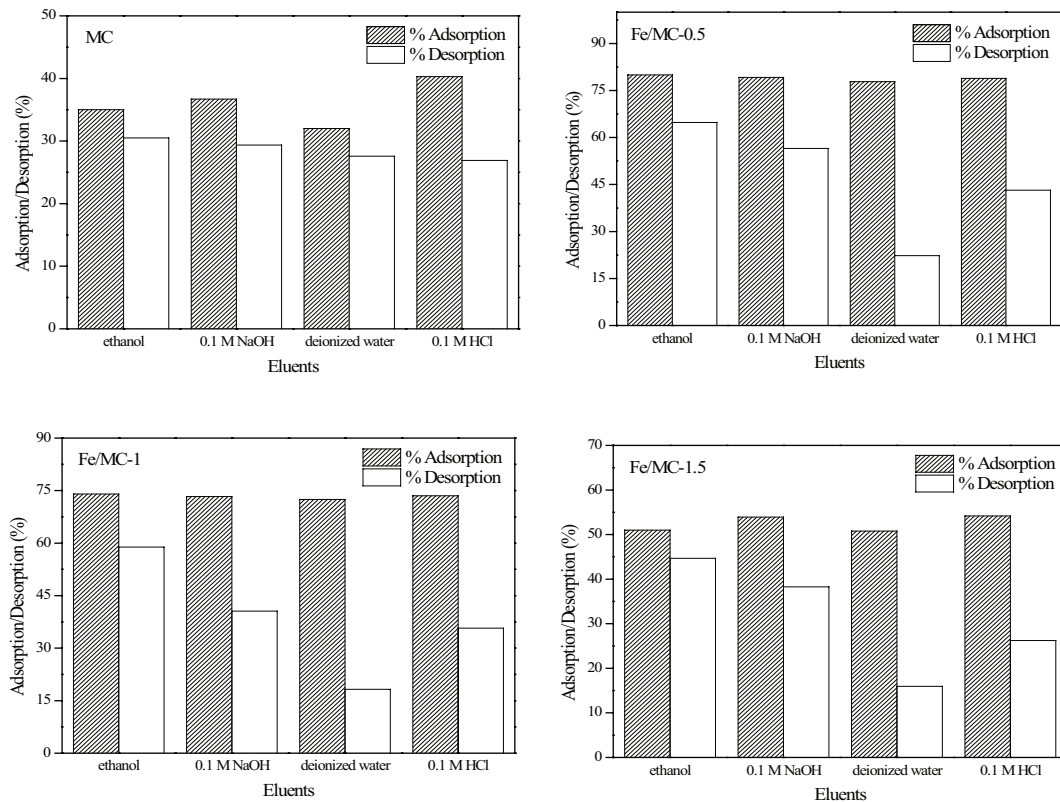


Fig. 10. Different desorption solutions for BPA adsorption.

Table 5  
Comparison of the monolayer adsorption capacity toward BPA with various adsorbents

Adsorbent	Adsorption capacity ( $Q_m$ , mg/g)	Reference
Biomass-based carbon modified with Fe	41.5	[72]
Biomass-based carbon with acid-washed	23.8	[72]
Biomass-based carbon modified with Ca	16.8	[72]
Single-walled carbon nanotubes (SWCNTs)	71	[24]
Multi-walled carbon nanotubes (MWCNTs)	111	[24]
Mesoporous carbon material (MC)	253.1	This study
Fe/MC-0.5	451.6	This study
Fe/MC-1	411.8	This study
Fe/MC-1.5	335.1	This study
MCM-41 mesoporous molecular sieves	416.7	[41]
MCM-41 modified with phenyltrimethoxysilane	351	[73]

thermodynamics analysis. According to equilibrium data, the adsorption equilibrium could be reached in 15–20 min and the kinetic modeling tends to follow the pseudo-second-order kinetic model which suggested adsorption mechanism lies in the electron sharing or electron transfer between the MC and Fe/MC and the BPA. The adsorption process is mainly chemisorption as the step of rate control. The results of adsorption isotherm analysis also indicate that multiple adsorption mechanisms coexist in the adsorption process. During the adsorption process of aromatic compounds and a large number of adsorbents,  $\pi$ -bonding is part of the adsorption

mechanism [74]. According to Fig. 5(b), it also can be found that the BPA might be adsorbed onto the MC and Fe/MC by hydrogen bonding or  $\pi$ - $\pi$  stacking interactions. Therefore, the adsorption mechanism is mainly chemisorption of hydrogen bonding or  $\pi$ - $\pi$  stacking interactions.

#### 4. Conclusions

(1) MC and Fe/MC were prepared via one-step hydrothermal synthesis method. The MC and Fe/MC showed a high specific surface area (644, 636, 636, 587 m<sup>2</sup>/g).

Modification made the Fe<sup>0</sup> exist in the synthesized composites, and with the amount of iron increasing, the content of iron in the synthesized composites increased, the order is reduced.

(2) The adsorbent dose (10–30 mg), initial concentration (20–100 mg/L), contact time (1–180 min) and reaction temperature (25°C–45°C) were evaluated, the result showed that the equilibrium adsorption capacity was negatively related to the adsorbent dosage, and positively correlated with the initial concentration. The maximum adsorption capacities of the MC and Fe/MC were 253.1, 451.6, 411.8, 335.1 mg/g, respectively, and the adsorption equilibrium could be reached in 15–20 min. Among them, the Fe/MC-0.5 possessed adsorption capacities of 451.6 mg/g and removal efficiency of 78.8%.

(3) The equilibrium data of MC and Fe/MC were perfectly accorded with the Freundlich isotherm. The kinetic modeling tends to follow the pseudo-second-order model. In addition, the adsorption process was spontaneous exothermic reaction, mainly dominated by both physical adsorption and chemisorption. The adsorption mechanism is mainly chemisorption of hydrogen bonding or  $\pi$ - $\pi$  stacking interactions.

### Acknowledgments

This study was supported by the Major National Science and Technology Projects of China (Grant No. 2016ZX05040–003) and Top Talents Project of China University of Petroleum (Grant No. 2015011). Authors are also grateful to Dr F. Liu for checking English phrasing of the manuscript.

### References

- [1] J. Li, J.L. Si, Introduction of environmental endocrine disruptors, *J. Environ. Health*, 16 (2002) 139–144.
- [2] T. Colborn, F.S. Vom Saal, A.M. Soto, Developmental effect of endocrine-disrupting chemicals in wildlife and humans, *Environ. Health Perspect.*, 101 (1993) 378–384.
- [3] Z.Y. Xue, Current situation and prospect of bisphenol A production process technology, *Chem. Eng. Res. Des.*, 16 (2006) 7–12.
- [4] A. Kumar, M. Naushad, A. Rana, Inammuddin, Preeti, ZnSe-WO<sub>3</sub> nano-hetero-assembly stacked on Gum Ghatti for photo-degradative removal of Bisphenol A: Symbiose of adsorption and photocatalysis, *Int. J. Biol. Macromol.*, 104 (2017) 1172–1184.
- [5] F. Ng, G. Couture, C. Philippe, S. Caillol, Bio-based aromatic epoxy monomers for thermoset materials, *Molecules*, 22 (2017) 149.
- [6] P. Dhiman, N. Mu, K.M. Batoo, A. Kumar, G. Sharma, Nano Fe<sub>3</sub>Zn<sub>1-x</sub>O as a tuneable and efficient photocatalyst for solar powered degradation of bisphenol A from aqueous environment, *J. Clean. Prod.*, 165 (2017) 1542–1556.
- [7] S.X. Gong, X.L. Wang, W. Liu, W. M.L. Wang, X. Wang, Aminosilanized magnetic carbon microspheres for the magnetic solid-phase extraction of bisphenol A, bisphenol AF, and tetrabromobisphenol A from environmental water samples, *J. Sep. Sci.*, 40 (2017) 1755–1764.
- [8] J. Goscianska, M. Marciniak, R. Pietrzak, Ordered mesoporous carbons modified with cerium as effective adsorbents for azo dyes removal, *Sep. Purif. Technol.*, 154 (2015) 236–245.
- [9] S. Nasser, S. Ebrahimi, M. Abtahi, R. Saeedi, Synthesis and characterization of polysulfone/graphene oxide nano-composite membranes for removal of bisphenol A from water, *J. Environ. Manage.*, 205 (2018) 174–182.
- [10] M. Alimohammadi, M. Askari, M. Dehghani, A. Dalvand, R. Saeedi, K. Yetilmessoy, B. Heibati, G. McKay, Elimination of natural organic matter by electrocoagulation using bipolar and monopolar arrangements of iron and aluminum electrodes, *Int. J. Environ. Sci. Technol.*, 14 (2017) 2125–2134.
- [11] A.A. Alqadami, M. Naushad, Z.A. Allothman, A.A. Ghfar, Novel metal-organic framework (MOF) based composite material for the sequestration of U(VI) and Th(IV) metal ions from aqueous environment, *ACS Appl. Mater. Interfaces*, 9 (2017) 36026–36037.
- [12] B. Manna, Rational functionalization of reduced graphene oxide with imidazole group for the electrochemical sensing of bisphenol A—an endocrine disruptor, *Analyst*, 143 (2018) 3451–3457.
- [13] J.F. Mora, G.J. Van Berkel, C.G. Enke, R.B. Cole, M. Martinez-Sanchez, Electrochemical processes in electrospray ionization mass spectrometry, *Mass Spectrom.*, 35 (2015) 939–952.
- [14] H. Kuramitz, M. Matsushita, S. Tanaka, Electrochemical removal of bisphenol A based on the anodic polymerization using a column type carbon fiber electrode, *Water Res.*, 38 (2004) 2331–2338.
- [15] K. Amit, K. Ajay, S. Gaurav, A. Ala' H, N. Mu, G. Ayman A., G. Changsheng, Biochar-templated g-C<sub>3</sub>N<sub>4</sub>/Bi<sub>2</sub>O<sub>3</sub>CO<sub>3</sub>/CoFe<sub>2</sub>O<sub>4</sub> nano-assembly for visible and solar assisted photo-degradation of paraquat, nitrophenol reduction and CO<sub>2</sub> conversion, *J. Chem. Eng.*, 339 (2018) 393–410.
- [16] Y.M. Kim, H.G. Song, Effect of fungal pellet morphology on enzyme activities involved in phthalate degradation, *J. Microbiol.*, 47 (2009) 420–424.
- [17] M.K. Ji, A.N. Kabra, J. Choi, J.H. Hwang, J.R. Kim, Biodegradation of bisphenol A by the freshwater microalgae *Chlamydomonas mexicana* and *Chlorella vulgaris*, *Ecol. Eng.*, 73 (2014) 260–269.
- [18] L. Mita, L. Grumiro, S. Rossi, C. Bianco, R. Defez, Bisphenol A removal by a *Pseudomonas aeruginosa* immobilized on granular activated carbon and operating in a fluidized bed reactor, *J. Hazard. Mater.*, 291 (2015) 129–135.
- [19] A.A. Al-Kahtani, T. Almuqati, N.A. Haqbani, T. hamad, M.N. Naushad, A clean approach for the reduction of hazardous 4-nitrophenol using gold nanoparticles decorated multiwalled carbon nanotubes, *J. Clean. Prod.*, 191 (2018) 429–435.
- [20] A. Bhatnagar, I. Anastopoulos, Adsorptive removal of bisphenol A (BPA) from aqueous solution: a review, *Chemosphere*, 168 (2017) 885–902.
- [21] K. Naddafi, N. Rastkari, R. Nabizadeh, R. Saeedi, M. Gholami, Removal of 2, 4, 6-trichlorophenol from aqueous solutions by cetylpyridinium bromide (CPB)-modified zeolite in batch and continuous systems, *Desal. Wat. Treat.*, 86 (2017) 131–138.
- [22] H. Liu, W. Peng, L.U. Jichang, F. Guo, Y. Luo, Research progress of fluoride-containing wastewater treatment by adsorption method, *Technol. Water Treat.*, 43 (2017) 13–18.
- [23] N. Mu, A. Ansari, M. Basheer, Al-Maswari, A.A. Alqadami, M. Saad, Alshehri, Nickel ferrite bearing nitrogen-doped mesoporous carbon as efficient adsorbent for the removal of highly toxic metal ion from aqueous medium, *J. Chem. Eng.*, 330 (2017) 1351–1360.
- [24] M.H. Dehghani, A.H. Mahvi, N. Rastkari, R. Saeedi, S. Nazmara, Adsorption of bisphenol A (BPA) from aqueous solutions by carbon nanotubes: kinetic and equilibrium studies, *Desal. Wat. Treat.*, 54 (2015) 84–92.
- [25] K. Mohanty, D. Das, M.N. Biswas, Preparation and characterization of activated carbons from Sterculia, alata, nutshell by chemical activation with zinc chloride to remove phenol from wastewater, *Adsorption*, 12 (2006) 119–132.
- [26] J. Goscianska, A. Olejnik, R. Pietrzak, Adsorption of l-phenylalanine on ordered mesoporous carbons prepared by hard template method, *J. Taiwan Inst. Chem. Eng.*, 45 (2014) 347–353.
- [27] J. Goscianska, A. Olejnik, R. Pietrzak, In vitro release of l-phenylalanine from ordered mesoporous materials, *Microporous Mesoporous Mater.*, 177 (2013) 32–36.
- [28] P. Elamathi, G. Chandrasekar, Pore size architecture of hexagonal mesoporous carbon nitride (HMCN) for metal-free synthesis of p-hydroxycinnamic acid, *Catal. Lett.*, 148 (2018) 1–10.

- [29] M. Ignat, M.E. Fortuna, L. Sacarescu, M.F. Zaltariov, V. Harabagiu, Pnipam-functionalized mesoporous carbon for the adsorption of vitamin B2, *J. Environ. Eng. Manage.*, 14 (2015) 607–613.
- [30] A.A. Alqadami, N. Mu, M.A. Abdalla, T. Ahamad, Z.A. Allothman, Efficient removal of toxic metal ions from wastewater using a recyclable nanocomposite: a study of adsorption parameters and interaction mechanism, *J. Clean. Prod.*, 156 (2017) 426–436.
- [31] M. Marciniak, J. Goscianska, R. Pietrzak, Physicochemical characterization of ordered mesoporous carbons functionalized by wet oxidation, *J. Mater. Sci.*, 53 (2018) 5997–6007.
- [32] J. Goscianska, A. Olejnik, I. Nowak, M. Marciniak, R. Pietrzak, Ordered mesoporous silica modified with lanthanum for ibuprofen loading and release behavior, *Eur. J. Pharm. Biopharm.*, 94 (2015) 550–558.
- [33] H. Li, H.A. Xi, S. Zhu, Z. Wen, R. Wang, Preparation, structural characterization, and electrochemical properties of chemically modified mesoporous carbon, *Microporous Mesoporous Mater.*, 96 (2016) 357–362.
- [34] S.M. Alshehri, M. Naushad, T. Ahamad, Z.A. Allothman, A. Aldalbahi, Synthesis, characterization of curcumin based ecofriendly antimicrobial bio-adsorbent for the removal of phenol from aqueous medium, *J. Chem. Eng.*, 254 (2014) 181–189.
- [35] Y. Huang, H. Cai, D. Feng, D. Gu, Y. Deng, One-step hydrothermal synthesis of ordered mesostructured carbonaceous monoliths with hierarchical porosities, *Chem. Commun.*, 23 (2008) 2641–2643.
- [36] J. Wang, H. Liu, J. Diao, X. Gu, H. Wang, Size-controlled nitrogen-containing mesoporous carbon nanospheres by one-step aqueous self-assembly strategy, *J. Mater. Chem.*, 3 (2015) 2305–2313.
- [37] S. Feng, R. Xu, New materials in hydrothermal synthesis, *Acc. Chem. Res.*, 34 (2001) 239–247.
- [38] D.Y. Zhao, Q.S. Huo, J.L. Feng, Nonionic triblock and star diblock copolymer and oligomeric surfactant syntheses of highly ordered, hydrothermally stable, mesoporous silica structures, *J. Am. Chem. Soc.*, 120 (1998) 6024–6036.
- [39] C.K. Choi, K.Y. Chung, T.Y. Lee, Direct modification method for strains due to non-conforming modes, *Struct. Eng. Mech.*, 11 (2001) 325–340.
- [40] L. Liu, F.Y. Wang, G.S. Shao, Z.Y. Yuan, A low-temperature autoclaving route to synthesize monolithic carbon materials with an ordered mesostructure, *Carbon*, 48 (2010) 2089–2099.
- [41] X. Liu, Y. Hu, J. Huang, C. Wei, Detailed characteristics of adsorption of bisphenol A by highly hydrophobic MCM-41 mesoporous molecular sieves, *Res. Chem. Intermediat.*, 42 (2016) 7169–7183.
- [42] J. Wei, Y. Liang, X. Zhang, G.P. Simon, D. Zhao, Controllable synthesis of mesoporous carbon nanospheres and Fe-N/carbon nanospheres as efficient oxygen reduction electrocatalysts, *Nanoscale*, 7 (2015) 6247–6254.
- [43] K.S.W. Sing, Reporting physisorption data for gas/solid systems with special reference to the determination of surface area and porosity, *Pure Appl. Chem.*, 57 (1985) 603–619.
- [44] P.A. Monson, P.A., Understanding adsorption/desorption hysteresis for fluids in mesoporous materials using simple molecular models and classical density functional theory, *Microporous Mesoporous Mater.*, 160 (2012) 47–66.
- [45] M. Li, Y.L. Wang, D. Liu, Q.Y. Li, X.S. Cong, Pore size-controlled synthesis of molecular sieves and their difference in catalytic properties for Fischer–Tropsch synthesis, *Appl. Petrochem. Res.*, 8 (2015) 1–6.
- [46] C. Liang, M. Kruk, A family of ordered mesoporous carbons derived from mesophase pitch using ordered mesoporous silicas as templates, *Adsorption*, 16 (2010) 465–472.
- [47] L. Liu, Q.F. Deng, B. Agula, X. Zhao, T.Z. Ren, Ordered mesoporous carbon catalyst for dehydrogenation of propane to propylene, *Catal. Commun.*, 16 (2011) 81–85.
- [48] J. Li, J. Gu, H. Li, Y. Liang, Y. Hao, X. Sun, L. Wang, Synthesis of highly ordered Fe-containing mesoporous carbon materials using soft templating routes, *Microporous Mesoporous Mater.*, 128 (2010) 144–149.
- [49] H. Jalili, N.F. Heinig, K.T. Leung, Formation of nanocrystalline films of  $\text{Sr}_2\text{FeMoO}_6$  on Si (100) by pulsed laser deposition: observation of preferential oriented growth, *J. Appl. Phys.*, 105 (2009) 1488.
- [50] S. Nam, P.G. Tratnyek, Reduction of azo dyes with zero-valent iron, *Water Res.*, 34 (2000) 1837–1845.
- [51] Y. Guo, D.A. Roekstraw, Physical and chemical properties of carbons synthesized from xylan, cellulose, and Kraft lignin by  $\text{H}_2\text{PO}_4$  activation, *Carbon*, 44 (2006) 1464–1475.
- [52] P.E. Fanning, M.A. Vannice, A DRIFTS study of the formation of surface groups on carbon by oxidation, *Carbon*, 31 (1993) 721–730.
- [53] P.S. Kumar, S. Ramalingam, C. Senthamarai, M. Niranjana, P. Vijayalakshmi, Adsorption of dye from aqueous solution by cashew nut shell: studies on equilibrium isotherm, kinetics and thermodynamics of interactions, *Desalination*, 261 (2010) 52–60.
- [54] I. Bautistatoledo, M.A. Ferrogarcía, J. Riverautrilla, Bisphenol A removal from water by activated carbon. Effects of carbon characteristics and solution chemistry, *Environ. Sci. Technol.*, 39 (2005) 6246–6250.
- [55] L.J. Kennedy, J.J. Vijaya, G. Sekaran, K. Kayalvizhi, Equilibrium, kinetic and thermodynamic studies on the adsorption of m-cresol onto micro- and mesoporous carbon, *J. Hazard. Mater.*, 149 (2007) 134–143.
- [56] I.A.W. Tan, A.L. Ahmad, B.H. Hameed, Adsorption of basic dye using activated carbon prepared from oil palm shell: batch and fixed bed studies, *Desalination*, 225 (2008) 13–28.
- [57] Y. Ren, W. Ma, J. Ma, Q. Wen, J. Wang, Synthesis and properties of bisphenol A molecular imprinted particle for selective recognition of BPA from water, *J. Colloid Interface Sci.*, 367 (2012) 355–361.
- [58] X. Jing, W. Li, Y. Zhu, Decontamination of bisphenol A from aqueous solution by graphene adsorption, *Langmuir*, 28 (2012) 8418–8425.
- [59] X. Zhou, J. Wei, K. Liu, K. Liu, N. Liu, B. Zhou, Adsorption of bisphenol A based on synergy between hydrogen bonding and hydrophobic interaction, *Langmuir*, 30 (2014) 13861–13868.
- [60] A.S. Alzaydien, Adsorption of methylene blue from aqueous solution onto a low-cost natural Jordanian Tripoli, *Am. J. Environ. Sci.*, 6 (2009) 1047–1058.
- [61] A.M. Joglekar, A.T. May, Product excellence through design of experiment, *Cereal Food World*, 32 (1987) 857–868.
- [62] F. Liu, Y.X. Dai, S. Zhang, J. Li, Z.C. Zhao, Modification and application of mesoporous carbon adsorbent for removal of endocrine disruptor bisphenol A in aqueous solutions, *J. Mater. Sci.*, 53 (2018) 2337–2350.
- [63] B.B. Cunha, W.G. Botero, L.C. Oliveira, V.M. Carlos, M.L.M. Pompeo, Kinetics and adsorption isotherms of bisphenol A, estrone, 17 $\beta$ -estradiol, and 17 $\alpha$ -ethinylestradiol in tropical sediment samples, *Water Air Soil. Pollut.*, 223 (2012) 329–336.
- [64] F. Liu, Y. Gao, S. Zhang, X. Yan, F.F. Fan, Application of mesoporous carbon and modified mesoporous carbon for treatment of DMF sewage, *J. Nanopart. Res.*, 18 (2016) 1–12.
- [65] J. Goscianska, M. Ptaszowska, R. Pietrzak, Equilibrium and kinetic studies of chromotrope 2R adsorption onto ordered mesoporous carbons modified with lanthanum, *J. Chem. Eng.*, 270 (2015) 140–149.
- [66] S. Biniak, G. Szymanski, J. Siedlewski, A. Swiqtowski, The characterization of activated carbons with oxygen and nitrogen surface groups, *Carbon*, 35 (1997) 1799–1810.
- [67] M. Iram, C. Guo, Y.P. Guan, A. Ishfaq, H.Z. Liu, Adsorption and magnetic removal of neutral red dye from aqueous solution using  $\text{Fe}_3\text{O}_4$  hollow nanospheres, *J. Hazard. Mater.*, 181 (2010) 1039–1050.
- [68] S. Zhang, F. Liu, J.M. Li, C. Zhang, Y. Gao, Synthesis of N-modified mesoporous carbon and the adsorption performance for nonylphenol ethoxylates from water, *Acta Petrolei Sinica (Petroleum Processing Section)*, 33 (2017) 471–479.
- [69] K. Naddafi, N. Rastkari, R. Nabizadeh, R. Saeedi, M. Gholami, M. Sarkhosh, Adsorption of 2, 4, 6-trichlorophenol from aqueous solutions by a surfactant-modified zeolitic tuff: batch and continuous studies, *Desal. Wat. Treat.*, 57 (2016) 5789–5799.

- [70] J. Goscińska, M. Marciniak, R. Pietrzak, Mesoporous carbons modified with lanthanum (III) chloride for methyl orange adsorption, *J. Chem. Eng.*, 247 (2014) 258–264.
- [71] B.V. Oepen, W. Kördel, W. Klein, Sorption of nonpolar and polar compounds to soils: processes, measurements and experience with the applicability of the modified OECD-Guideline 106, *Chemosphere*, 22 (1991) 285–304.
- [72] R. Juhola, H. Runtti, T. Kangas, T. Hu, H. Romar, S. Tuomikoski, Bisphenol A removal from water by biomass-based carbon: Isotherms, kinetics and thermodynamics studies, *Environ. Technol.*, 117 (2018) 1–10.
- [73] Y. Kim, B. Lee, K. Choo, S. Choi, Selective adsorption of bisphenol A by organic–inorganic hybrid mesoporous silicas, *Microporous Mesoporous Mater.*, 138 (2011) 184–190.
- [74] G. Zhao, L. Jiang, Y. He, J. Li, H. Dong, Sulfonated graphene for persistent aromatic pollutant management, *Adv. Mater.*, 23 (2011) 3959–3963.